

**DEPENDENCE OF ESCAPE FRACTION OF ULTRAVIOLET
RADIATION ON GALAXY MASS**

A Thesis
Presented to
The Academic Faculty

by

Vasiliy Grigoriyovich Demchenko

In Partial Fulfillment
of the Requirements for the Degree
Bachelor of Science in Physics in the
School of Physics

Georgia Institute of Technology
May 2013

COPYRIGHT 2013 BY VASILIIY GRIGORIYVICH DEMCHENKO

**DEPENDENCE OF ESCAPE FRACTION OF ULTRAVIOLET
RADIATION ON GALAXY MASS**

Approved by:

Dr. John Wise, Advisor
School of Physics
Georgia Institute of Technology

Dr. David Ballantyne
School of Physics
Georgia Institute of Technology

Dr. Brian Kennedy
School of Physics
Georgia Institute of Technology

Date Approved: 04/26/2013

ACKNOWLEDGEMENTS

I wish to thank Dr. John Wise, Assistant Professor of the School of Physics at The Georgia Institute of Technology, for his mentorship and patience throughout my undergraduate research career. I would also like to thank my mother and father for their constant support and unfaltering belief in my success.

TABLE OF CONTENTS

	Page
ACKNOWLEDGEMENTS	iv
LIST OF SYMBOLS AND ABBREVIATIONS	vi
SUMMARY	vii
<u>CHAPTER</u>	
1 Introduction	1
2 Methods and Materials	3
Enzo: An Adaptive Mesh Refinement Code	3
Simulation Details	5
3 Results	7
Outflow Visualization	7
Escape Fraction Dependence	8
Higher Time Fidelity Analysis	13
4 Discussion & Conclusion	16
REFERENCES	19

LIST OF SYMBOLS AND ABBREVIATIONS

M_*	Stellar Mass
f_{gas}	Gas Fraction
M_{200}	Halo Mass
f_{star}	Star Formation Efficiency
κ	Absorption Coefficient
c	Speed of Light
f_{esc}	Photon Escape Fraction
n_H	Hydrogen Number Density
β_2	Recombination Coefficient
ρ_o	Density
R_{200}	Virial Radius
H_o	Hubble Constant
G	Gravitational Constant
Ω_b	Baryon Mass Fraction
z	Redshift
R_s	Strömgren Radius
t_H	Hubble Time
L_γ	Photon Number Luminosity
$N_{\gamma,esc}$	Number of Escaped Photons
f_γ	Stellar Efficiency

SUMMARY

Using the N-body, adaptive mesh-refinement, ray-tracing code Enzo, we studied the escape fraction of ultraviolet radiation in the early universe. We obtained data from a simulated cube 1 Mpc across of the early universe during the period known as reionization. We studied the effects of various galaxy properties on the escape fraction of ionizing radiation over a redshift period of $7.2 < z < 15$. Using the data, we looked at all-sky maps of the neutral hydrogen and electron density at approximately 637 million years after the Big Bang. We found that the ionizing radiation escapes anisotropically from dark matter halos. We then studied the how the escape fraction of ionizing radiation depends on dark matter halo mass. We found that the escape fraction begins to decrease as a function of mass. This led us to conclude that high-mass, high-luminosity galaxies are not a main source of ionizing radiation. Since these high-mass, high-luminosity galaxies are created when low-mass galaxies combine, we conclude that it is in fact low-mass, low-luminosity galaxies that are the dominant contributors of ionizing radiation. They are more abundant and have higher escape fractions of radiation, thus supporting our claim. We also looked at finer time fidelity for the last 80 million years of the simulation to discover more about the escape fraction of radiation. We found that the escape fraction can vary over short timesteps of several million years, which is short in the cosmological sense. We compared our findings to those of Hinshaw et al. 2012 for their nine-year WMAP data. Their findings show an epoch of reionization at a redshift of approximately $z = 10$. Our results suggest that the main drivers of this reionization are the low-luminosity galaxies that we have studied in this thesis.

CHAPTER 1

INTRODUCTION

In the time following the Dark Ages, approximately 150 to 800 million years after the Big Bang, when the only radiation was from the 21 cm hydrogen line, came a period of reionization. Stars began to form and radiate, thus creating enough radiation energy to ionize neutral hydrogen. In order for hydrogen to be ionized photons must have an energy of 13.6 eV or greater. This type of energy radiates in the ultraviolet (UV) portion of the electromagnetic spectrum. Previous research [Bouwens et al. 2004] has shown that a strong source of this reionization is the formation and evolution of high redshift galaxies. Redshift, z , is a measure of how distant an object in the universe is from the current time denoted by $z = 0$. For example, the redshift of the Cosmic Background Radiation as found by Fixsen et al. 1994 is approximately $z = 1089$, which corresponds to 379,000 years after the Big Bang. This redshift-time relation can be found in Bergström & Goobar's *Cosmology and Particle Astrophysics* (Eq. 4.79). As these galaxies form, radiation can affect the outer regions of the galaxies by heating and ionizing it, thus creating an H II region (for simplification we assume only the ionization of hydrogen).

This thesis focuses on the amount of UV radiation that escapes from these early galaxies as they form. It is important to understand what fraction of the radiation actually escapes in order to further understand this period of reionization. Previous research has shown that approximately 10% of the hydrogen ionizing radiation escapes galaxies and this had been thought to be true for all galaxies. However, more recent research has shown drastically different results. New research has shown that in early dwarf galaxies the escape fraction of radiation can be up to 80% [Wise & Cen 2009]. This discovery fosters more questions that need to be researched and are the reason for this thesis.

Previous research [Alvarez et al. 2006] has simulated a single Population III star (Pop III stars contains no elements heavier than lithium) and its effects upon the surrounding H II region. This research suggests that the escape fraction is dependent on the stellar mass and that the higher the mass, the greater the escape fraction over time. Furthermore, the greater the initial mass of the star, the greater the ionizing luminosity over time. This creates a larger H II region. The same approach is taken in this paper, but with several distinct differences. Instead of analyzing simulations containing Pop III stars of mass $M \sim 60M_{sun}$ at a redshift of $z = 20$, we studied young (< 20 million years) Pop II (metal enriched) stars at redshifts ranging from $7.2 < z < 15$. Furthermore, instead of studying single stars and their effects, we studied whole galaxies that contain these young stars and compared the results with those of Alvarez et al. 2006. Since these were early galaxies, they are considered dwarf galaxies and do not behave in the same fashion as larger galaxies [Wise & Cen 2008]. Also, instead of using the simulation code GADGET, we implemented the use of Enzo, an adaptive mesh refinement cosmological code. This code solves both Poisson's equation and Euler's equations of hydrodynamics and uses ray tracing techniques to transport radiation. We will specifically focus on how the ionization of hydrogen affect the escape fraction and the star formation in galaxies, where does most of this radiation escape from, what effect does it have on the surroundings, and how quickly this process occurs.

CHAPTER 2

METHODS AND MATERIALS

Enzo: An Adaptive Mesh Refinement Code

The simulations that were used in this research are created by the radiation hydrodynamics code Enzo. Enzo is an Eulerian block-structured adaptive mesh refinement code for cosmological purposes [O’Shea et al. 2004]. This code solves N-body dynamics via the particle-mesh technique, and it follows the physics in highly accurate manner. For example, using the fast fourier transform (FFT) and multigrid techniques, the Poisson equation is solved. Furthermore, with the aid of a modified piecewise parabolic method (PPM), Euler’s equation of hydrodynamics is solved. Other physics packages, such as set methods for star formation, UV background, and a myriad of radiative cooling techniques, add to the accuracy of the code’s simulations. These techniques are used to artificially recreate how a representative portion of the universe evolves with time.

Enzo was created to avoid problems encountered when attempting to resolve large scale objects such as galaxies. Using a single grid to resolve galaxies at approximately five orders of magnitude of dynamical range can be costly, whereas smooth particle hydrodynamics lacks in accuracy of shock and fixed mass resolution. Grid-based techniques using adaptive mesh refinement reduces these problems greatly and allows for higher-order hydrodynamics schemes. Since the universe is filled with dark matter, it constitutes a large portion of the large scale dynamics. Instead of using the Boltzmann equation as a model for dark matter (and other collisionless particles) and considering it as a second fluid, Enzo uses an N-body method instead. This method follows trajectories of individual particles controlled by the following coupled equations.

$$\frac{dx_p}{dt} = v_p \quad (1)$$

$$\frac{dv_p}{dt} = -\nabla\phi \quad (2)$$

In the previous equations, x_p is the particle position, v_p is the particle velocity, and $-\nabla\phi$ is the gravitational force term. For simplicity, equations 1 and 2 are shown without cosmological terms. A solution to these equations can be found in solving the Poisson equation:

$$\nabla^2\phi = 4\pi G\rho \quad (3)$$

The density, ρ , takes into account both collisionless fluid (particles) and collisional fluid (baryonic gas). The hydrodynamics implemented in Enzo are detailed by Bryan et al. 1995, however the main features are discussed here. A non-linear Riemann solver and a version of Godunov’s method are used in order to solve shock capturing. A Friedman-Robertson-Walker spacetime in co-moving coordinates is used for the conservation of fluid mass, momentum, and energy. Both the spacetime and Riemann solver are modified to include gravity. In order to limit inaccuracies in regards to pressures and temperatures of baryon gas, Enzo solves both the total energy and internal gas energy equations everywhere on each grid, at all times. This method ensures proper entropy jumps at strong shocks and furthermore yields accurate temperatures and pressures in the hypersonic flows, known as *dual energy formalism* [O’Shea et al. 2004].

Enzo also uses adaptive ray tracing techniques as described by Wise & Abel 2011. Ray tracing is used to propagate radiation from a point source on a computational grid. This method is only accurate if there are a sufficient number of rays passing through each cell. Along the ray, the radiative transfer equation is as follows:

$$\frac{1}{c} \frac{\partial P}{\partial t} + \frac{\partial P}{\partial r} = -\kappa P \quad (4)$$

In this equation, P is the photon flux along the ray. The ray tracing technique that is used [Abel & Wandelt 2002] progressively splits rays when the sampling of them becomes too coarse. This splitting is based on a technique called Hierarchical Equal Area isoLatitude Pixelation (HEALPix). In this method, the rays are traced along normal directions of the centers of HEALPix pixels that divide a sphere into equal areas. The rays are then initialized at each point source with a photon luminosity equally spread across a number of rays determined by the initial HEALPix level [Wise & Abel 2011]. The ray propagates and splits until one of several criteria causes it to cease splitting. For a further

discussion of ray tracing and its coupling with the AMR code Enzo, refer to Wise & Abel 2011.

Simulation Details

The calculations of escape fraction in comparison to various variables were run with python scripts using the YT module. YT is a data analysis program designed for astrophysical simulations. The program includes conveniences such as volume rendering, splicing, and plotting. Since its focus is for astrophysics, the basic units are cgs and other variables are also set such that they align with astrophysical data. The toolkit also takes into account multiple physical phenomena such as the accelerated expansion of the universe and the redshift due to that expansion. This particular data set simulated a cube 1 Mpc across (1 pc = 3.26 light years). The star forming regions were followed over a time period of 775 million years and the data was analyzed every 12.5 million years. As previously mentioned, this simulation is analyzed from a redshift $z = 15$ to a redshift $z = 7.2$. We calculated the escape fraction by tracing rays from each star particle to the virial radius of the halo using 768 rays, which corresponds to a HEALPix level 3. We compute the total neutral hydrogen column density, from which we can calculate the fraction of radiation that escapes from the galaxy itself.

Since the execution of the code requires a large amount of computer memory, it could not be run in a timely manner using a regular computer. The Georgia Institute of Technology's computer cluster was remotely accessed in order to compile the code and obtain the data. The cluster used is called "Cygnus" and took approximately three days for the computer to run the code for all of the data sets and graphs. The code is written to be run in parallel so that more than one core could be used to compile it. This method accelerates its execution. In this particular case, 4 cores and 24 GB of memory were used and the data collection took several days for each run. Due to several setbacks such as YT updates and miscalculations in the code itself, this compilation process was needed to be conducted several times throughout the research process. This method helped acquire the data necessary to investigate the escape fraction of radiation as compared to the star formation rate, total halo mass, and total stellar mass. Upon the initial inspection of the data, it has been concluded that in order to obtain a better understanding of the escaping radiation, the behavior of the escape fraction with respect to time and halo mass at a

higher time fidelity was necessary. The simulation was re-executed with finer time resolution for the last 80 million years of the simulation. This simulation was restarted when the universe was 650 million years old. From these data, the following graphs were created: escape fraction versus halo mass, escape fraction versus time, and halo mass versus time. Scatter plots of star efficiency multiplied by escape fraction versus halo mass, escape fraction versus halo mass, and escape fraction versus stellar mass were also created for the full simulations spanning all the redshifts previously discussed.

CHAPTER 3

RESULTS

Outflow Visualization

In order to better understand how radiation was escaping from the galaxy, it would be beneficial to visualize it. We used all-sky maps with the observer at the galaxy center to aid in our interpretation. The following figures show all-sky maps show the electron fraction and neutral hydrogen fraction, respectively. They are for the third most massive dark matter halo of the simulation when the universe was 637.5 million years old.

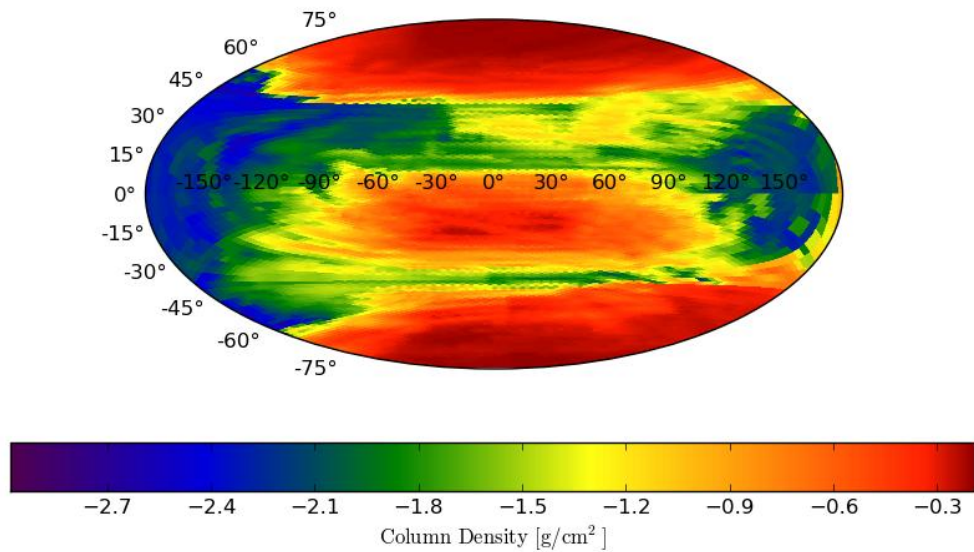


Figure 1: All-sky map for electron fraction of the third most massive dark matter halo that has a total and stellar mass of $7.25 \times 10^7 M_{sun}$ and $2.46 \times 10^4 M_{sun}$, respectively. The age of the universe at this point in the simulation is 687.5 million years old and the column density is on a log scale.

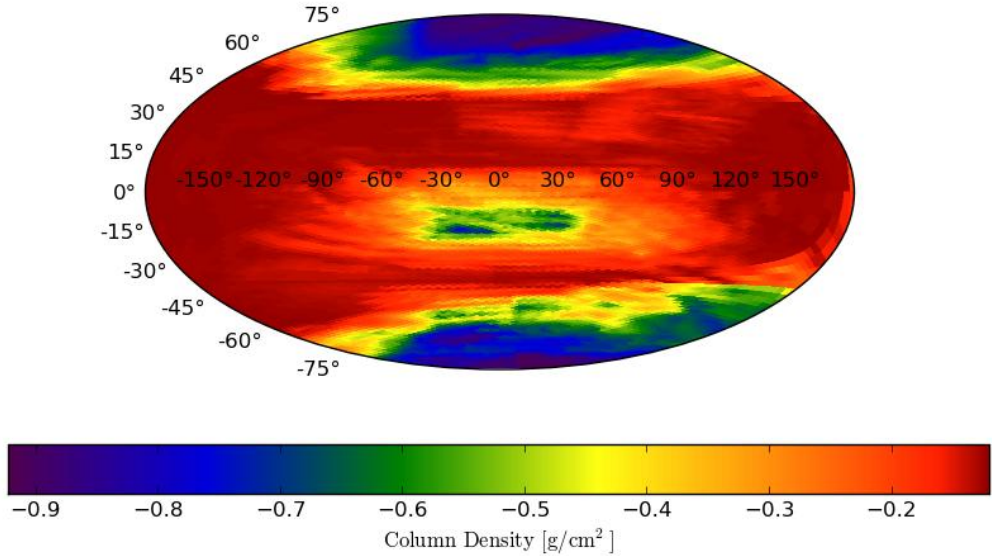


Figure 2: All-sky map for neutral hydrogen fraction of the third most massive dark matter halo that has a total and stellar mass of $7.25 \times 10^7 M_{sun}$ and $2.46 \times 10^4 M_{sun}$, respectively. The age of the universe at this point in the simulation is 687.5 million years old and the column density is on a log scale.

The most important aspect to note is that the electron fraction is highest where the neutral hydrogen is least dense. These are the areas where radiation escapes from the dark matter halo and, consequently, the galaxy. Similar to the outflows of a black hole, the radiation due to the galaxy in this halo mainly escapes from the poles of the galaxy. In this case, the outflow can be visualized to create a polar outflow of radiation as is the case for most disk shaped galaxies. This will help to visually understand the process that is occurring when we discuss escaping radiation in subsequent sections.

Escape Fraction Dependence

As previously mentioned, the goal of this study was to observe whether the escape fraction of radiation from dark matter halos has any dependence on various properties of the halo. The escape fraction is defined as the fraction of ionizing photons that escape from the halo compared to those that do not escape. In this study, the properties investigated are stellar and halo mass. The following two figures show log-linear scatter

plots of the escape fraction of radiation versus stellar mass and escape fraction versus dark matter halo mass, respectively. The data for Figure 3 was obtained using the galaxy mass exclusively due to Pop II stars that are younger than 20 million years from the simulation.

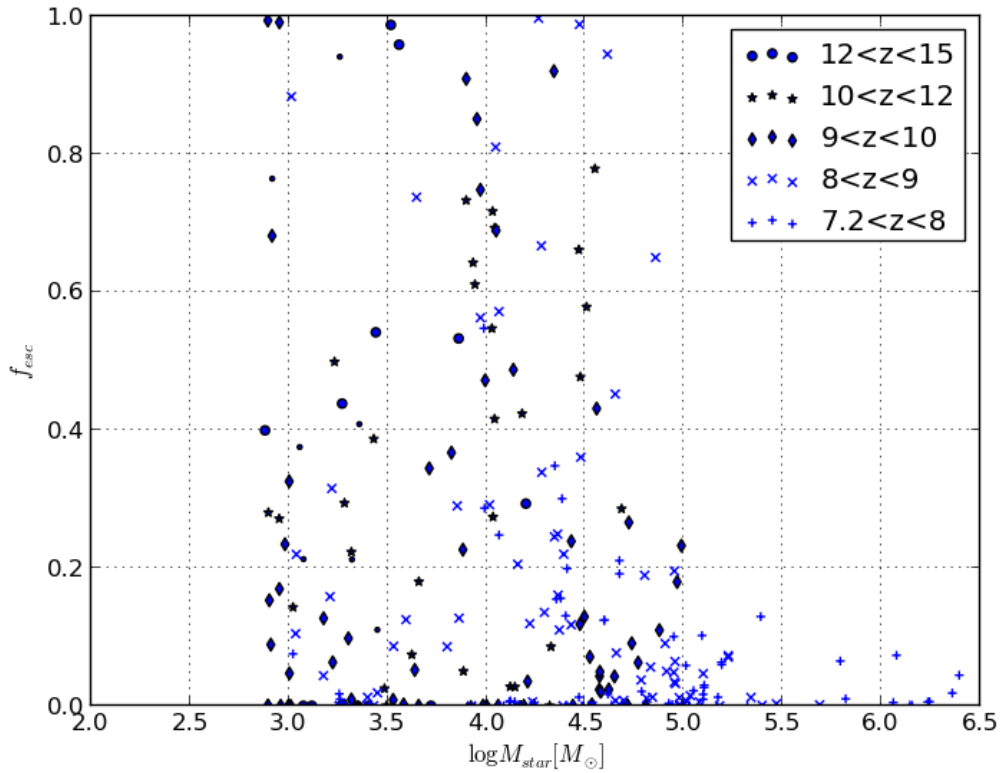


Figure 3: A scatter plot of escape fraction of radiation versus the log of stellar mass (in solar mass units). The plot shows variation of escape fraction not only for various masses, but also for various redshifts. Note that the galaxies with the highest stellar mass are the ones with the least radiation escaping from them and are also the ones with the lowest redshift.

The plot also covers five redshift ranges as well as mass. As the graph suggests, the lowest redshift gives the highest stellar mass, which have the lowest escape fraction. We see that the majority of the escape fraction comes from galaxies having a stellar mass of 10^3 - $10^5 M_{sun}$ and that the higher mass dwarf galaxies contribute very little to the escape fraction.

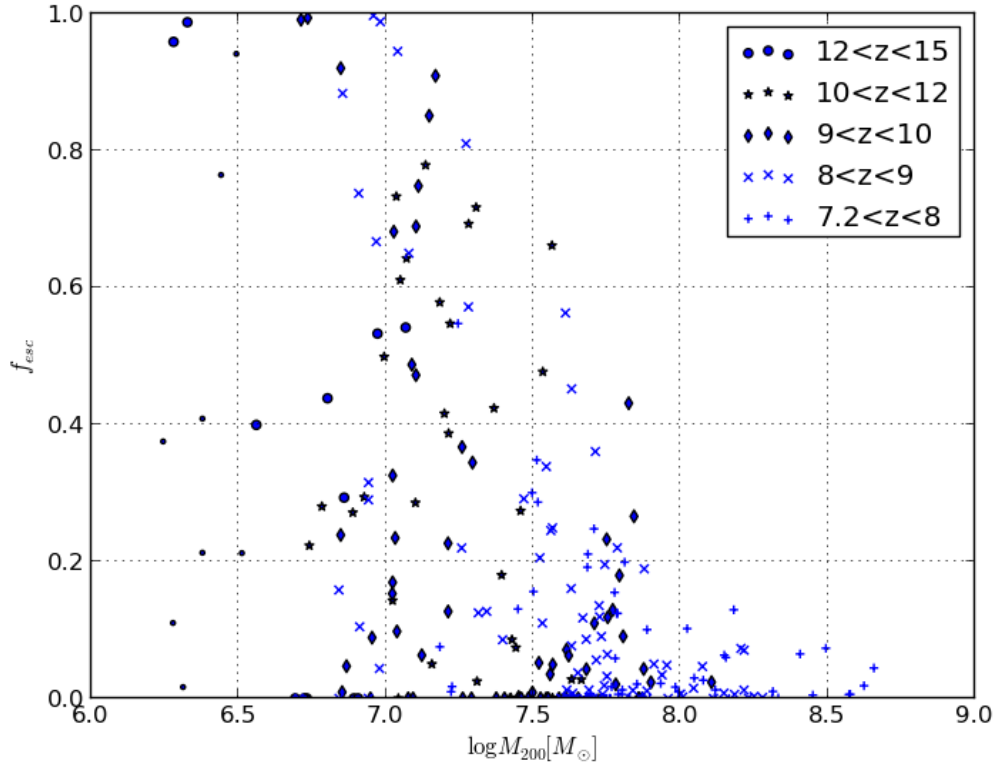


Figure 4: A scatter plot of escape fraction of radiation versus the log of dark matter halo mass (in solar mass units). The plot shows variation of escape fraction not only for various masses, but also for various redshifts. Note that the highest mass stars are the ones with the least radiation escaping from them and are also the ones with the lowest redshift.

As with the stellar mass plot, the dark matter halo mass plot shows a similar dependence. One difference is that the dark matter halo mass plot does not show a distinct mass cutoff, like the stellar mass plot shows, but a smooth transition to a low escape fraction. Since these plots have a large scatter, no analytical fit was made to them. However, such was not the case for the graph in Figure 5. This figure shows a scatter plot of the product of star formation efficiency (star formation rate per unit gas) and escape fraction of radiation versus dark matter halo mass.

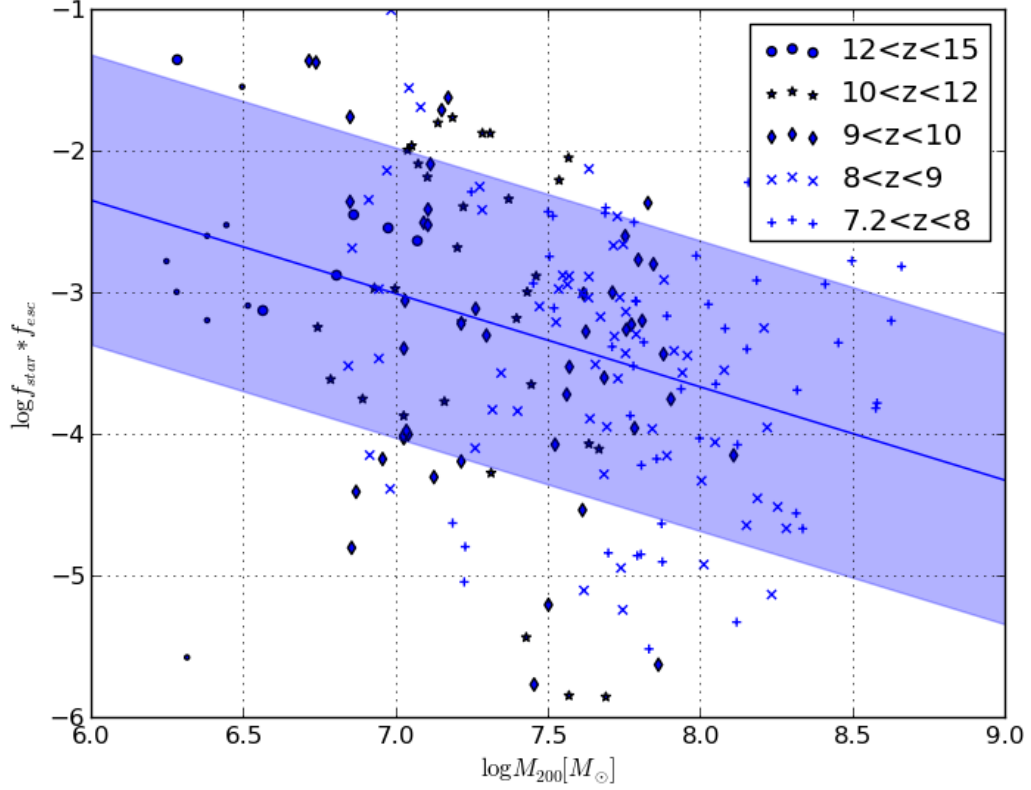


Figure 5: A log-log scatter plot of the product of the escape fraction of radiation with star formation efficiency versus dark matter halo mass. The highest mass halos are mostly found to be at the lower redshifts (as with the previous plots).

Unlike the previous plots, the plot in Figure 5 is on a log-log scale. Upon inspection, it was found that this plot has a pattern so a linear relation was fit to the data. The curve was fit as a linear relation with a slope of $m = -0.659 \pm 0.018$ and a y-intercept of $b = 1.610 \pm 1.026$. In order to properly fit this curve, a minimum $f_{star} * f_{esc}$ was needed to be obtained in order to disregard outliers. The following sets of equations describe how the minimum $f_{star} * f_{esc}$ was found. We begin with the definition of Strömgen Radius and density:

$$R_s = \left(\frac{3L_\gamma}{4\pi n_H^2 \beta_2} \right)^{1/3} \quad (5)$$

$$\rho_o = \frac{3H_o^2}{8\pi G} (1+z) \quad (6)$$

For this particular calculation, a value of $z = 7$ was used. The values for the Hubble Constant, H_o , and the Gravitational Constant, G , are $2.3 \times 10^{-18} \text{ s}^{-1}$ and $6.67 \times 10^{-11} \text{ m}^3 \text{ kg}^{-1} \text{ s}^{-2}$, respectively. Furthermore, we also know the equation for the virial radius, R_{200} . We can solve for it by assuming the Strömngren Radius has to be greater than the virial radius in order to have radiation escape from the dark matter halo. We can therefore solve Eq. (7) and set it equal to Eq. (5) in order to obtain the minimum luminosity, L_γ , of the galaxy for radiation to escape.

$$R_{200} = \left(\frac{3M_{200}}{200\rho_o 4\pi} \right)^{1/3} \quad (7)$$

We can solve Eq. (7) knowing that $M_{200} = 10^8 M_{sun}$. By replacing R_s with R_{200} , we can solve for L_γ knowing that $\beta_2 = 2 \times 10^{-19} \text{ s}^{-1}$ and $n_H = 133 \text{ m}^{-3}$ from the following relation:

$$n_H = \frac{\rho_o}{m_H} \Omega_b \quad (8)$$

Where $m_H = 1.67 \times 10^{-27} \text{ kg}$, ρ_o is found from the relation in Eq. (6), and $\Omega_b = 0.0449$.

Therefore, rearranging Eq. (5) we solve that $L_\gamma = 2.188 \times 10^{45} \text{ s}^{-1}$ from the relation in Eq. (9).

$$L_\gamma = \frac{4\pi n_H^2 \beta_2 R_{200}^3}{3} \quad (9)$$

Knowing the luminosity, we can calculate the number of escaped photons by multiplying the luminosity by the Hubble Time, $t_H = 700$ million years. From Eq. (10) and (11), we can rearrange to find a relationship for $f_{star} * f_{esc}$.

$$N_{\gamma,esc} = M_* f_\gamma f_{esc} \quad (10)$$

$$M_* = f_{gas} M_{200} f_{star} \quad (11)$$

Assuming that $f_{gas} = 0.1$ and $f_\gamma = 6000$, we can use Eq. (12) to find that

$$f_{star} * f_{esc} = 6.7 \times 10^{-7}.$$

$$f_{esc} * f_{star} = \frac{N_{\gamma,esc}}{f_\gamma f_{gas} M_{200}} \quad (12)$$

Using this value as a baseline, a curve could be fit through the data above this value of $f_{star} * f_{esc}$ as seen in Figure 5. The errors to the curve were also graphed as seen with the blue shaded region. The error in the slope of the curve was neglected when the errors were graphed. Notice that both in Figures 4 and 5 there is a distinct decrease in the

escape fraction and the product of escape fraction and star formation efficiency as halo mass increases.

Higher Time Fidelity Analysis

For the finer time resolution results, the data for the last 80 million years of the simulation were closely studied. As can be seen from Figures 6 and 7, there was evidently a burst of star formation at 665 million years, whose massive stars died 20 million years later. This burst creates a spike in the escape fraction during this period. Then, we see a sudden drop in both the galaxy mass and the escape fraction. This is presumably a supernova, or some other high energy event, which blows out mass from the halo.

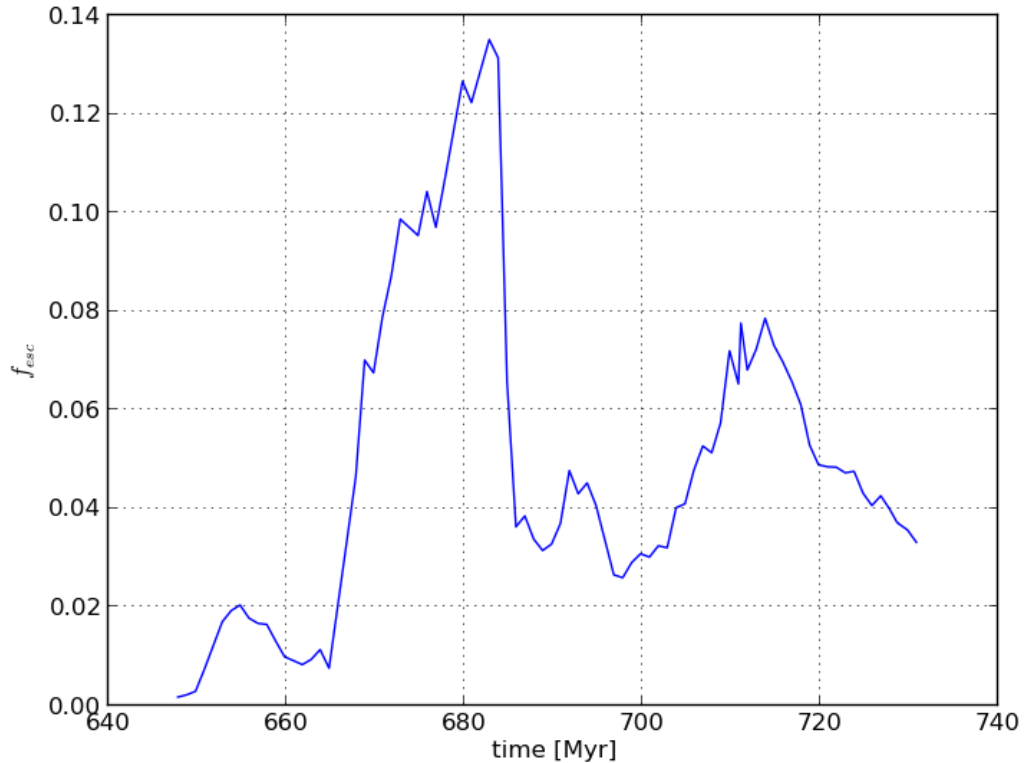


Figure 6: A graph of the escape fraction as a function of time for the last 80 million years of the simulation.

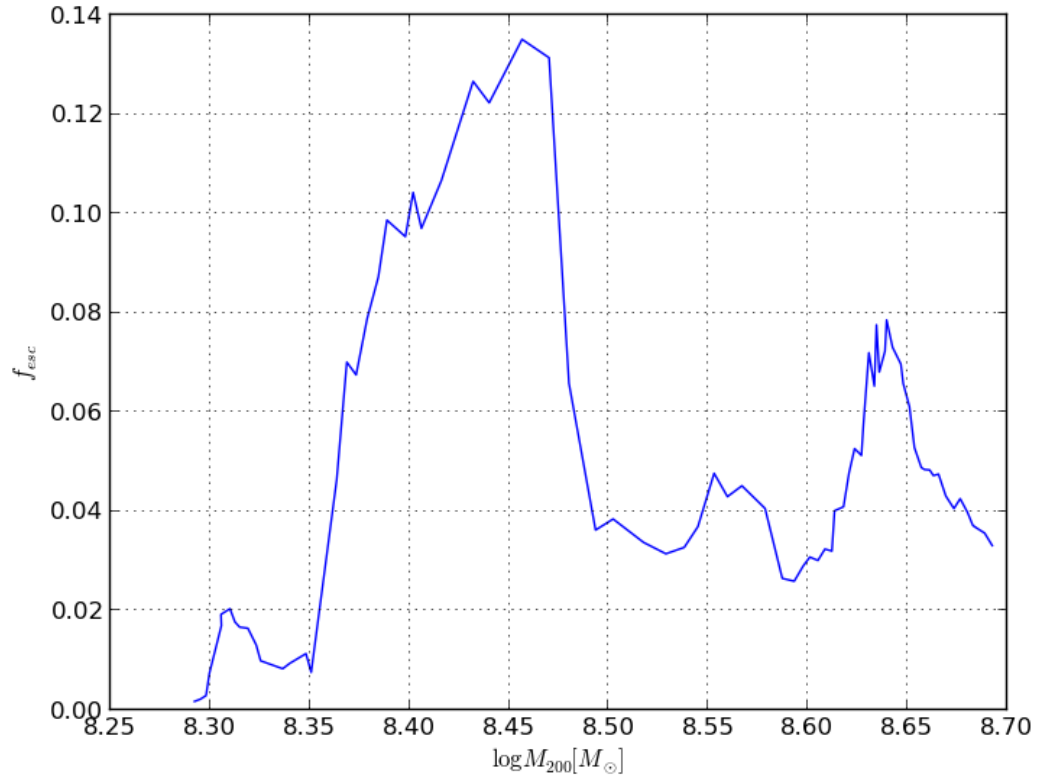


Figure 7: A graph of the escape fraction as a function of dark matter halo mass for the last 80 million years of the simulation.

The similarities in the graphs of Figures 6 and 7 are expected. Since the galaxy is growing in mass over time, there are more objects to create radiation, thus the escape fraction increases as a function of both galaxy mass and time between 665 and 685 million years. The following figure shows a graph of this mass over time dependence.

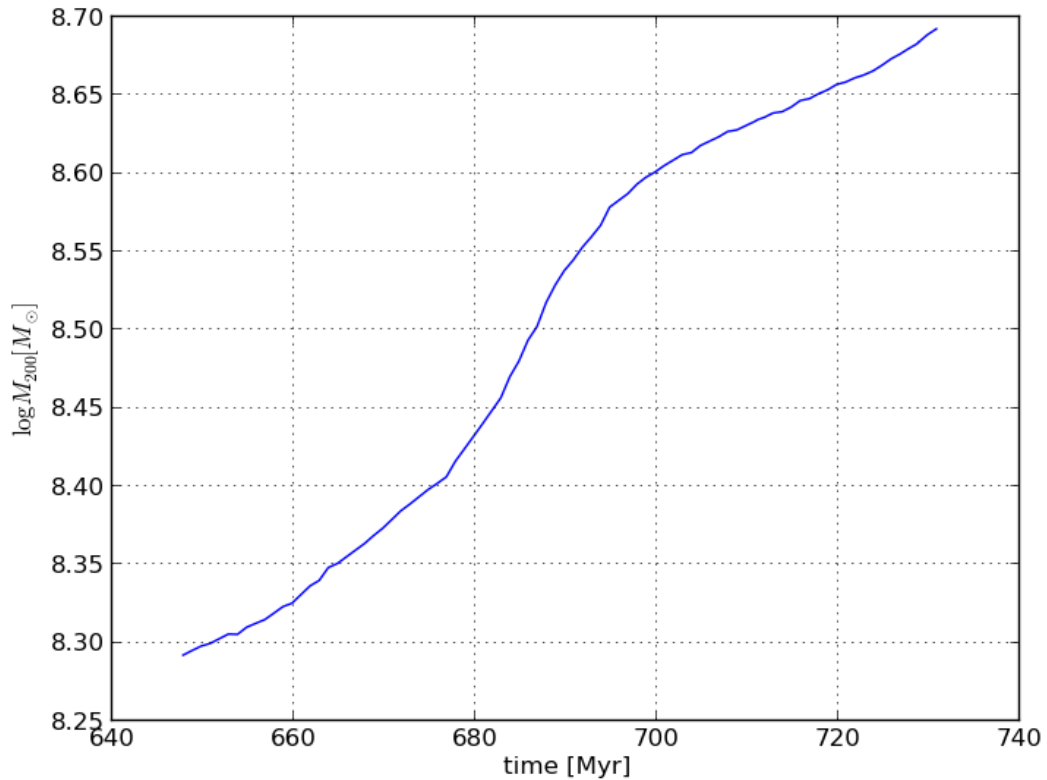


Figure 8: A graph of the dark matter halo as a function of time for the last 80 million years of the simulation.

In Figure 8 there is a clear increase of halo mass as a function of time. We also see an increase in the halo mass accretion, starting at 680 million years, creating a “s-shaped” curve instead of a linear one. This accretion event sparks another burst of star formation that is also seen in the increase of the escape fraction. The process begins again at approximately 700 million years, however this time we see that the escape fraction is not as high as it was before. There are several things that can alter this. One reason is that not as many stars are being formed during this cycle since some of the material could have been blown out in the previous supernova.

CHAPTER 4

DISCUSSION & CONCLUSION

Using the N-body, adaptive mesh refinement, ray-tracing code Enzo, we successfully studied and analyzed a cosmological simulation, which covered a volume of 1 Mpc^3 and spanned 775 million years. In this simulation, we followed the effects that Pop II stars that are 20 million years or younger have on their host galaxy. The evolution of these stars and the galaxies were investigated in a redshift range of $7.2 < z < 15$. Our goal was to study the escape fraction of ionizing radiation and its dependence on various properties such as dark matter halo mass and stellar mass. Taking a snapshot at approximately 637 million years, we looked at the third most massive dark matter halo with a total mass of $7.25 \times 10^7 M_{sun}$ and a stellar mass of $2.46 \times 10^4 M_{sun}$ to see where the ionizing radiation was escaping from via an all-sky map. We see that the ionized regions coincide with the lowest column densities of neutral hydrogen. As seen in Figures 1 and 2, most of the ionizing radiation is escaping from the poles; however that is not always the case. In fact, further studies of other dark matter halos all-sky maps, we found that the ionizing radiation escapes from the halo in anisotropic manner.

Next, we found and analyzed the dependence of the escape fraction of ionizing radiation as a function of stellar mass and dark matter halo mass. We also investigated the dependence of the product of escape fraction of radiation with the star formation efficiency. The galaxies that were studied in all three of these experiments contained Pop II (metal-enriched) stars whose ages were 20 million years or less. As can be seen from the scatter plot in Figure 4, there is a clear dependence of the escape fraction of ionizing radiation decreasing as a function of dark matter halo mass. In some cases, such as where the halo mass is $\sim 10^{7.75}$ and greater, the escape fraction is only 0.1 or less. This means that large mass halos are not the primary source of reionization in this redshift range. From this we conclude that the main sources of reionization are the low-mass (low-luminosity) galaxies because we see that they have a higher escape fraction of radiation. To further show that the main source of ionizing photons comes from low-mass galaxies, we look at the results of Reed et al. 2007. We look at the dark matter halos whose mass is greater than $10^8 M_{sun}$ since radiation of the halos with a lower mass does not allow them

to cool enough to form stars, thus $f_{esc} = 0$. At this halo mass Reed et al. 2007 has shown that the number density of halos (n_{halo}) is inversely proportional to the halo mass (M_{200}). We also see from Figure 5 that $f_{star} * f_{esc}$ is proportional to $M_{200}^{-0.7}$. With these relations, we can approximate the total number density of photons per unit volume

$n_{\gamma} = n_{halo} * M_{200} * f_{gas} * f_{\gamma} * f_{star} * f_{esc}$. Considering f_{gas} and f_{γ} as being constant (like in section 3), we see that n_{γ} is proportional to $M_{200}^{-0.7}$. From this, we can conclude that the majority of ionizing radiation comes from the low-mass galaxies. Moreover, we also know that formation of large-mass halos occurs hierarchically, meaning that small-mass halos combine to form these large-mass halos. In this well-established model, we deduce that the abundance of small-mass halos is larger than that of large-mass ones. This dominance in abundance, alongside a higher escape fraction of ionizing radiation, brings us to the conclusion that it is the small-mass halos that dominate reionization. This conclusion is further reinforced by the scatter plot in Figure 5 where we see a clear decrease of the product of the escape fraction of radiation with the star formation efficiency. This plot confirms our findings that the main contributors to reionization are high-redshift, low-mass dark matter halos.

The next step was to look at a higher time resolution of the data for the more massive, dwarf galaxies. We studied the last 80 million years of the simulation and observed the behavior of the escape fraction of radiation in more detail. We see that the escape fraction evolves with time in a similar fashion that halo mass is evolving with time as shown in Figures 6 and 7. The reason that we see a burst of escape fraction during the stellar formation is due to the gradual expansion of the H II region. As stars form, their photons ionize the gas around them creating an ever-growing H II region. Over time, the combination of all the stellar formation in the galaxy make the H II region grow larger than the dark matter halo itself. This “break out” of the H II region is the reason we see ionizing radiation escape from halos during star formation. It is interesting to see that the escape fraction can vary on such a short cosmological timesteps as seen in Figure 6. As we have already noted, the escape fraction of radiation is relatively low in during this time, it does not get much above 0.13. We also note that there is some periodic increase in the escape fraction as we see galaxies producing in a bursting manner. We further note that the galaxies do not produce the same amount of stars

during each cycle since some of the material is blown out due to supernovae, stellar winds, and various other factors.

In a recent study by Hinshaw et al. 2012, the nine-year WMAP observations were used to further study the fundamental cosmological model and the conditions of the early universe. In their study they found the redshift for the reionization period to be approximately $z = 10$ as can be found in Table 2 of Hinshaw et al. 2012. Using the data in this thesis, it can be suggested that it is the low-luminosity, low-mass galaxies that are a key component in this epoch of reionization. Galaxies at this redshift contributed a significant amount to the escape fraction of reionization as seen from Figures 3 and 4. We suggest that future research should focus on these low-luminosity galaxies; particularly paying attention to the ones with a redshift $z \geq 10$. Further research on this topic will significantly help us understand the period of reionization and the early universe as a whole.

REFERENCES

- [1] Abel, Tom, and Benjamin D. Wandelt. "Adaptive Ray Tracing for Radiative Transfer around Point Sources." *Monthly Notices of the Royal Astronomical Society* 330.3 (2002): *Arxiv.org*. Cornell University Library, 01 Nov. 2001. Web. 23 Mar. 2013.
- [2] Bergström, L., Goobar, A. (2006). *Cosmology and Particle Astrophysics* (2 ed.). Springer. p. 77, Eq.4.79.
- [3] Bouwens, R. J., G. D. Illingworth, R. I. Thompson, J. P. Blakeslee, M. E. Dickinson, T. J. Broadhurst, D. J. Eisenstein, X. Fan, M. Franx, G. Meurer, and P. Van Dokkum. "Star Formation At~ 6: The Hubble Ultra Deep Parallel Fields." *The Astrophysical Journal* 606.1 (2004): L25-28.
- [4] Bryan, Greg L., Michael L. Norman, James M. Stone, Renyue Cen, and Jeremiah P. Ostriker. "A Piecewise Parabolic Method for Cosmological Hydrodynamics." *Computer Physics Communications* 89.1-3 (1995): 149-68.
- [5] Fixsen, D. J., E. S. Cheng, D. A. Cottingham, R. E., Jr. Eplee, R. B. Isaacman, J. C. Mather, S. S. Meyer, P. D. Noerdlinger, R. A. Shafer, R. Weiss, E. L. Wright, C. L. Bennett, N. W. Boggess, T. Kelsall, S. H. Moseley, R. F. Silverberg, G. F. Smoot, and D. T. Wilkinson. "Cosmic Microwave Background Dipole Spectrum Measured by the COBE FIRAS Instrument." *The Astrophysical Journal* 420.2 (1994): 445-49.
- [6] Hinshaw, G., et al. "Nine-Year Wilkinson Microwave Anisotropy Probe (WMAP) Observations: Cosmological Parameter Results." *Astrophysical Journal Supplement Series* (2012): 20 Dec. 2012.
- [7] Kim, Ji-Hoon, Mark R. Krumholz, John H. Wise, Matthew J. Turk, Nathan J. Goldbaum, and Tom Abel. "Dwarf Galaxies with Ionizing Radiation Feedback. II: Spatially-resolved Star Formation Relation." *Arxiv.org*. Cornell University Library, 25 Oct. 2012. Web. 29 Oct. 2012. <<http://arxiv.org/abs/1210.6988>>.
- [8] Kuhlen, M., Krumholz, M. R., Madau, P., Smith, B. D., & Wise, J. H. 2012, "Dwarf Galaxy Formation with H₂-regulated Star Formation", *Astrophysical Journal*, 749, 36-57.
- [9] O'Shea, Brian W., Greg Bryan, James Bordner, Michael Norman, Tom Abel, Robert Harkness, and Alexei Kritsuk. "Introducing Enzo, an AMR Cosmology Application." *Arxiv.org* (2004): *Cornell University Library*. Web. 23 Mar. 2013. <<http://arxiv.org/abs/astro-ph/0403044>>.

- [10] Reed, Darren S., Richard Bower, Carlos S. Frenk, Adrian Jenkins, and Tom Theuns. "The Halo Mass Function from the Dark Ages through the Present Day." *Monthly Notices of the Royal Astronomical Society* 374.1 (2007): 2-15.
- [11] Reiss, Adam G. "Observational Evidence from Supernovae for an Accelerating Universe and a Cosmological Constant." *The Astronomical Journal* 16.3 (1998)
- [12] Scoville, Nick Z. "Evolution of Star Formation and Gas." *Arxiv.org*. Cornell University Library, 25 Oct. 2012. Web. 29 Oct. 2012.
<<http://arxiv.org/abs/1210.6990>>.
- [13] Wise, John H., and Tom Abel. "Enzo+Moray: Radiation Hydrodynamics Adaptive Mesh Refinement Simulations with Adaptive Ray Tracing." *Monthly Notices of the Royal Astronomical Society* 414.4 (2011): 3458-491. *Arxiv.org*. Cornell University Library, 15 Mar. 2011. Web. 23 Mar. 2013.
- [14] Wise, J. H., Abel, T., Turk, M. J., Norman, M. L., & Smith, B. D. 2012, "The Birth of a Galaxy. II. The Role of Radiation Pressure", *Monthly Notices of the Royal Astronomical Society*
- [15] Wise, J. H., & Cen, R. 2009, "Ionizing Photon Escape Fractions from High Redshift Dwarf Galaxies," *Astrophysical Journal*, 693, 984-999
- [16] Wise, J. H., Turk, M. J., Norman, M. L., & Abel, T. 2012, "The Birth of a Galaxy: Primordial Metal Enrichment and Population II Stellar Populations", *Astrophysical Journal*, 745, 50-59

VITA

VASILY G. DEMCHENKO

DEMCHENKO was born in Moscow, Russia and moved to the United States of America in 1998 when he was 7 years old. He attended public school in Roswell, Georgia. He enrolled at The Georgia Institute of Technology in the fall of 2009. He graduated from The Georgia Institute of Technology with a Bachelors of Science in Physics in May of 2013. Upon graduation, he has accepted a job as a Radio Antenna Network Engineer with AT&T that he will start in July of 2013. In his spare time, Vasily is an avid music follower and enjoys playing his guitar. He enjoys the company of friends and family and always seeks to be surrounded by them.